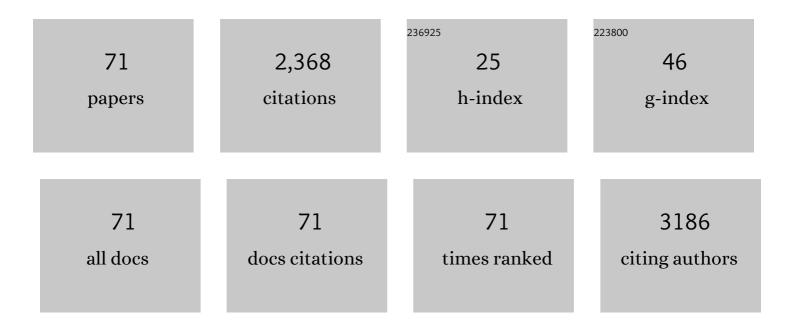
List of Publications by Year in descending order

Source: https://exaly.com/author-pdf/6807735/publications.pdf Version: 2024-02-01



#	Article	IF	CITATIONS
1	Large Two-Magnon Raman Hysteresis Observed in a Magnetically Uncompensated Hematite Coating across the Morin Transition. Coatings, 2022, 12, 540.	2.6	4
2	Photocontrolled Strain in Polycrystalline Ferroelectrics via Domain Engineering Strategy. ACS Applied Materials & Interfaces, 2021, 13, 20858-20864.	8.0	15
3	Ultrasensitive NO2 gas sensor with insignificant NH3-interference based on a few-layered mesoporous graphene. Sensors and Actuators B: Chemical, 2021, 335, 129657.	7.8	27
4	Wear behavior in pastes of alkali-activated materials: Influence of precursor and alkali solution. Tribology International, 2020, 147, 106293.	5.9	13
5	Preparation and Characterization of Large Area Li-NASICON Electrolyte Thick Films. Inorganics, 2019, 7, 107.	2.7	6
6	Preparation of nanostructured TiO2 films with high catalytic activity and their 3D spatial distribution of anatase and rutile phases. Journal of Materials Science, 2019, 54, 9414-9425.	3.7	6
7	Photo-Controlled Ferroelectric-Based Nanoactuators. ACS Applied Materials & Interfaces, 2019, 11, 13921-13926.	8.0	23
8	2D compositional self-patterning in magnetron sputtered thin films. Applied Surface Science, 2019, 480, 115-121.	6.1	3
9	The fight against multidrug-resistant organisms: The role of ZnO crystalline defects. Materials Science and Engineering C, 2019, 99, 575-581.	7.3	17
10	Structural insights of hierarchically engineered feldspars by confocal Raman microscopy. Journal of Raman Spectroscopy, 2019, 50, 741-754.	2.5	8
11	In situ full view of the Portland cement hydration by confocal Raman microscopy. Journal of Raman Spectroscopy, 2019, 50, 720-730.	2.5	28
12	Study of the Interface of the Early Stages of Growth under Quasiâ€Equilibrium Conditions of ZnO on Graphene/Cu and Graphite. Advanced Materials Interfaces, 2019, 6, 1801689.	3.7	6
13	Investigation of thermal stability of 2D and 3D CoAl2O4 particles in core-shell nanostructures by Raman spectroscopy. Journal of Alloys and Compounds, 2019, 779, 244-254.	5.5	41
14	Poling and depoling influence on the micro-stress states and phase coexistence in KNN-based piezoelectric ceramics. Journal of the European Ceramic Society, 2019, 39, 1011-1019.	5.7	15
15	Confocal Raman Microscopy Can Make a Large Difference: Resolving and Manipulating Ferroelectric Domains forÂPiezoelectric Engineering. Springer Series in Surface Sciences, 2018, , 531-556.	0.3	3
16	Fabrication of biocompatible and efficient antimicrobial porous polymer surfaces by the Breath Figures approach. Journal of Colloid and Interface Science, 2018, 513, 820-830.	9.4	17
17	Reversible optical control of macroscopic polarization in ferroelectrics. Nature Photonics, 2018, 12, 29-32.	31.4	97
18	Electric field effect on the microstructure and properties of Ba <sub>0.9</sub> Ca <sub>0.1</sub> Ti <sub>0.9</sub> Ca <sub>O.1</sub> Ti <sub>0.9</sub> Zr <sub>0.1</sub> O <sub>3</sub> (BCTZ) lead-free ceramics. Journal of Materials Chemistry A, 2018, 6, 5419-5429.	10.3	24

#	Article	IF	CITATIONS
19	Exploring new methodologies for the identification of the morphotropic phase boundary region in the (BiNa)TiO3-BaTiO3 lead free piezoceramics: Confocal Raman Microscopy. Journal of Alloys and Compounds, 2018, 739, 799-805.	5.5	22
20	Fabrication of 3D printed objects with controlled surface chemistry and topography. European Polymer Journal, 2018, 98, 21-27.	5.4	13
21	Experimental evidence of charged domain walls in lead-free ferroelectric ceramics: light-driven nanodomain switching. Nanoscale, 2018, 10, 705-715.	5.6	29
22	Improved conductivity in tape casted Li-NASICON supported thick films: Effect of temperature treatments and lamination. Journal of the European Ceramic Society, 2018, 38, 1679-1687.	5.7	18
23	Ag-AgO nanostructures on glass substrates by solid-state dewetting: From extended to localized surface plasmons. Journal of Applied Physics, 2018, 124, .	2.5	16
24	Light-Induced Capacitance Tunability in Ferroelectric Crystals. ACS Applied Materials & Interfaces, 2018, 10, 21804-21807.	8.0	28
25	Immobilization of Polyoxometalates on Tailored Polymeric Surfaces. Nanomaterials, 2018, 8, 142.	4.1	6
26	Honeycomb Films with Core–Shell Dispersed Phases Prepared by the Combination of Breath Figures and Phase Separation Process of Ternary Blends. Langmuir, 2017, 33, 2872-2877.	3.5	4
27	Thermoelectric Skutterudite/oxide nanocomposites: Effective decoupling of electrical and thermal conductivity by functional interfaces. Nano Energy, 2017, 31, 393-402.	16.0	34
28	Wrinkling and Folding on Patched Elastic Surfaces: Modulation of the Chemistry and Pattern Size of Microwrinkled Surfaces. ACS Applied Materials & Interfaces, 2017, 9, 20188-20195.	8.0	14
29	Switchable and pH responsive porous surfaces based on polypeptide-based block copolymers. Materials and Design, 2017, 131, 121-126.	7.0	16
30	Thermal Route for the Synthesis of Maghemite/Hematite Core/Shell Nanowires. Journal of Physical Chemistry C, 2017, 121, 23158-23165.	3.1	17
31	Epsilon iron oxide: Origin of the high coercivity stable low <scp>C</scp> urie temperature magnetic phase found in heated archeological materials. Geochemistry, Geophysics, Geosystems, 2017, 18, 2646-2656.	2.5	43
32	Highly Efficient Antibacterial Surfaces Based on Bacterial/Cell Size Selective Microporous Supports. ACS Applied Materials & Interfaces, 2017, 9, 44270-44280.	8.0	29
33	New insights in weathering analysis of anhydrous cements by using high spectral and spatial resolution Confocal Raman Microscopy. Cement and Concrete Research, 2017, 100, 119-128.	11.0	39
34	2D particles forming a nanostructured shell: A step forward cool NIR reflectivity for CoAl2O4 pigments. Dyes and Pigments, 2017, 137, 1-11.	3.7	62
35	Confocal Raman Microscopy: new perspective on the weathering of anhydrous cement. IOP Conference Series: Materials Science and Engineering, 2017, 251, 012035.	0.6	1
36	Origin of the magnetic transition at 100 K in <i>ε</i> -Fe <sub>2</sub> O <sub>3</sub> nanoparticles studied by x-ray absorption fine structure spectroscopy. Journal of Physics Condensed Matter, 2017, 29, 485701.	1.8	13

#	Article	IF	CITATIONS
37	Symmetry constraints during the development of anisotropic spinodal patterns. Scientific Reports, 2016, 6, 20806.	3.3	12
38	Synthesis and structural characterization of Zn <sub>x</sub> Fe <sub>3â^'x</sub> O <sub>4</sub> ferrite nanoparticles obtained by an electrochemical method. RSC Advances, 2016, 6, 40067-40076.	3.6	62
39	Modification of poly(dimethylsiloxane) as a basis for surface wrinkle formation: Chemical and mechanical characterization. Polymer, 2016, 98, 327-335.	3.8	20
40	Lithium La <sub>0.57</sub> Li <sub>0.33</sub> TiO <sub>3</sub> Perovskite and Li <sub>1.3</sub> Al <sub>0.3</sub> Ti <sub>1.7</sub> (PO <sub>4</sub> ) <sub>3</sub> Li-NASICON Supported Thick Films Electrolytes Prepared by Tape Casting Method. Journal of the Electrochemical Society, 2016, 163, A1653-A1659.	2.9	30
41	Enhancement of UV absorption behavior in ZnO–TiO2 composites. Boletin De La Sociedad Espanola De Ceramica Y Vidrio, 2016, 55, 55-62.	1.9	84
42	Sol–Gel Synthesis and Micro-Raman Characterization of ε-Fe <sub>2</sub> O <sub>3</sub> Micro- and Nanoparticles. Chemistry of Materials, 2016, 28, 511-518.	6.7	115
43	Fabrication of hierarchical wrinkled morphologies through sequential <scp>UVO</scp> treatments. Journal of Applied Polymer Science, 2015, 132, .	2.6	10
44	Stabilization of cubic phase in dense Eu2O3 ceramics. Materials Letters, 2015, 157, 77-80.	2.6	12
45	Influence of surface modifiers on hydrothermal synthesis of K x Na(1â^'x)NbO3. Journal of Materials Science: Materials in Electronics, 2015, 26, 9402-9408.	2.2	6
46	Nanopatterning on highly oriented pyrolytic graphite surfaces promoted by cobalt oxides. Carbon, 2015, 85, 89-98.	10.3	8
47	Indirect measurement of stress distribution in quartz particles embedded in a glass matrix by using confocal Raman microscopy. Ceramics International, 2015, 41, 13598-13606.	4.8	23
48	Tribochemical Decomposition of Light Ionic Hydrides at Room Temperature. Journal of Physical Chemistry Letters, 2015, 6, 2780-2785.	4.6	14
49	Poly(Ethylene Oxide) Functionalized Polyimide-Based Microporous Films to Prevent Bacterial Adhesion. ACS Applied Materials & Interfaces, 2015, 7, 9716-9724.	8.0	21
50	Ferroelectric domain wall motion induced by polarized light. Nature Communications, 2015, 6, 6594.	12.8	138
51	Revealing the role of cationic displacement in potassium–sodium niobate lead-free piezoceramics by adding W <sup>6+</sup> ions. Journal of Materials Chemistry C, 2015, 3, 4168-4178.	5.5	36
52	Lead-Free Piezoceramics: Revealing the Role of the Rhombohedral–Tetragonal Phase Coexistence in Enhancement of the Piezoelectric Properties. ACS Applied Materials & Interfaces, 2015, 7, 23080-23088.	8.0	122
53	A simple aqueous electrochemical method to synthesize TiO <sub>2</sub> nanoparticles. Physical Chemistry Chemical Physics, 2015, 17, 29319-29326.	2.8	18
54	Sintering behaviour and translucency of dense Eu2O3 ceramics. Journal of the European Ceramic Society, 2014, 34, 1803-1808.	5.7	19

#	Article	IF	CITATIONS
55	Influence of B-site compositional homogeneity on properties of (K0.44Na0.52Li0.04)(Nb0.86Ta0.10Sb0.04)O3-based piezoelectric ceramics. Journal of the European Ceramic Society, 2014, 34, 2249-2257.	5.7	16
56	Versatile Approach for the Fabrication of Functional Wrinkled Polymer Surfaces. Langmuir, 2014, 30, 13244-13254.	3.5	10
57	Tuning the Pore Composition by Two Simultaneous Interfacial Self-Assembly Processes: Breath Figures and Coffee Stain. Langmuir, 2014, 30, 6134-6141.	3.5	13
58	Formation of Multigradient Porous Surfaces for Selective Bacterial Entrapment. Biomacromolecules, 2014, 15, 3338-3348.	5.4	19
59	Characterization of Carbon Nanoparticles in Thin-Film Nanocomposites by Confocal Raman Microscopy. Journal of Physical Chemistry C, 2014, 118, 10488-10494.	3.1	16
60	High Strain in (K,Na)NbO <sub>3</sub> -Based Lead-Free Piezoelectric Fibers. Chemistry of Materials, 2014, 26, 3838-3848.	6.7	79
61	Inorganic hydrophobic coatings: Surfaces mimicking the nature. Ceramics International, 2013, 39, 2489-2495.	4.8	23
62	Fabrication of Structured Porous Films by Breath Figures and Phase Separation Processes: Tuning the Chemistry and Morphology Inside the Pores Using Click Chemistry. ACS Applied Materials & Interfaces, 2013, 5, 3943-3951.	8.0	37
63	Quantum Speed Limits in Open System Dynamics. Physical Review Letters, 2013, 110, 050403.	7.8	356
64	Resolution of the ferroelectric domains structure in (K,Na)NbO3-based lead-free ceramics by confocal Raman microscopy. Journal of Applied Physics, 2013, 113, .	2.5	25
65	Chemical Analysis with High Spatial Resolution by Rutherford Backscattering and Raman Confocal Spectroscopies: Surface Hierarchically Structured Glasses. Journal of the American Ceramic Society, 2013, 96, 1783-1788.	3.8	13
66	High spatial resolution structure of (K,Na)NbO3 lead-free ferroelectric domains. Journal of Materials Chemistry, 2012, 22, 9714.	6.7	97
67	Ordered arrays of polymeric nanopores by using inverse nanostructured PTFE surfaces. Nanotechnology, 2012, 23, 385305.	2.6	10
68	Hierarchically Structured Multifunctional Porous Interfaces through Water Templated Self-Assembly of Ternary Systems. Langmuir, 2012, 28, 9778-9787.	3.5	44
69	Isolated NAnoparticle Raman Spectroscopy. Journal of Raman Spectroscopy, 2012, 43, 889-894.	2.5	22
70	Dielectric behaviour of Hf-doped CaCu3Ti4O12 ceramics obtained by conventional synthesis and reactive sintering. Journal of the European Ceramic Society, 2012, 32, 1691-1699.	5.7	46
71	Block Copolymer Surfactants in Emulsion Polymerization: Influence of the Miscibility of the Hydrophobic Block on Kinetics, Particle Morphology, and Film Formation. Macromolecules, 2011, 44, 4282-4290.	4.8	35